The impact of modified rate of precipitation conversion parameter in the convective parameterization scheme of operational weather forecast model (GFS T1534) over Indian summer monsoon region

Malay Ganai[1], Snehlata Tirkey[1], R.P.M. Krishna[1] and P. Mukhopadhyay[1]

[1]Indian Institute of Tropical Meteorology, Pune, India

Prediction of Indian summer Monsoon in GFS T1534

Cloud condensate to precipitation conversion parameter

Improved prediction of moderate and heavy rainfall in EXPT over Indian region

Corresponding author: Dr. P. Mukhopadhyay

IITM, Dr.Homi Bhabha Road, Pashan, Pune 411008

Email: mpartha@tropmet.res.in

Telephone:+91 20 25904221

FAX: +91 20 25865142

Abstract

The performance of present operational global forecast system (GFS) at T1534 (~12.5 km) horizontal resolution with modified fractional cloud condensate to precipitation conversion parameter in the simplified Arakawa-Schubert (SAS) convection scheme is evaluated for the summer monsoon seasons of 2018 and 2019 over the Indian region. The modified parameter has the form of an exponential decreasing function of temperature above the freezing level, whereas below the freezing level, it is constant and similar to default conversion parameter. The results reveal that the GFS T1534 with modified conversion parameter (EXPT) shows better fidelity in forecasting the mean summer monsoon rainfall over the Indian continent region as compared to default GFS T1534 (CTRL). The rainfall probability distribution function analysis indicates notable improvement in forecasting moderate and heavier category rainfall in EXPT as compared to CTRL. The improved distribution of total rainfall is found be contributed by the proper forecasting of convective and large-scale rainfall in EXPT. It is likely that the reduced rate of conversion of cloud condensate to convective precipitation above the freezing level leads to decrease in convective rainfall, which eventually increases the moisture in the upper level through detrainment and hence enhancement in large-scale rainfall. Further, EXPT shows relative improvement in forecasting outgoing longwave radiation, wind circulation, cloud fraction, dynamical-thermodynamical processes and moist-convective feedback through better lower tropospheric moistening over the Indian region. Finally, various skill score analyses suggest that EXPT shows better skill in predicting moderate and heavier category rainfall with longer lead time over the continental Indian region. Considering the large socio-economic impact of heavy and extreme precipitation over India, the modified conversion parameter can be incorporated in the present operational GFS T1534 model.

1. Introduction

Reliable prediction of summer monsoon precipitation is crucial for agriculture, water resource management, and many other socioeconomic aspects (Gadgil & Gadgil 2006).The skill of the numerical weather prediction models is improved over the years primarily due to better initialization, increased resolution and advanced model physics. In spite of this, the simulation of proper spatio-temporal distribution of monsoon rainfall and its variabilities remains a challenging task to the research community (Waliser et al., 2003; Lin et al., 2008; Sperber & Annamalai 2008). Several studies have been carried out to simulate the Indian summer monsoon (ISM) from Atmospheric Global Circulation Models (AGCMs) (Sperber & Palmer 1996; Gadgil & Sajani 1998; Sabre et al., 2000; Waliser et al., 2003; Abhik et al., 2014) as well as Coupled ocean-atmosphere Global Circulation Models (CGCMs) (Yang et al., 2008; Pattanaik & Kumar 2010; Kim et al., 2012; Saha et al., 2013; Ramu et al., 2016). In spite of better skill in CGCMs, all the above studies unanimously showed prominent dry bias over the Indian subcontinent in both the atmospheric and coupled GCMs.

Several studies (Manabe et al., 1970; Mahlman & Urnscheid (1987); Kiehl & Williamson (1991); Williamson et al., (1995); Hack et al., (2006); Rajendran & Kitoh (2008); Manganello et al., 2012; Mukhopadhyay et al., 2019) have pointed out the importance of model resolution in simulating various aspects of the atmospheric fields. Majority of these studies emphasized the importance of higher resolution models for better representation of orography, land-ocean coastlines, vegetation cover, land use and associated nonlinear processes. Manganello et al., (2012) highlighted that the track and intensity of tropical cyclone is well predicted by 10 km European Centre for Medium Range Weather Forecast (ECMWF) Integrated Forecast System (IFS) model as compared to coarser resolution IFS.In recent decades, a lot of progress has been

made in terms of resolution of the operational forecasting model mainly due to advancement in computing facilities throughout the globe. Recently, ECMWF incorporates a very high resolution GCM (9 km for deterministic and 18 km for ensemble forecast) for 10 days weather prediction (https://www.ecmwf.int/en/forecasts/documentation-and-support). While the extreme rainfall over the Indian subcontinent shows an increasing trend (Goswami et al., 2006; Rajeevan et al., 2008; Roxy et al., 2017). Kim et al., (2018) demonstrated the importance of high resolution models in simulating extreme precipitation over Indian region. Further, Trenberth et al., (2012) indicated that the climate models have a tendency to produce more frequent but less intense rain than observed heavy rainfall.

Over the Indian region, the operational medium range forecast started at National Centre for Medium Range Weather Forecast (NCMRWF) in 1994 using the T80L18 global data assimilation and forecasting system. With the gradual progress in observing data network, data assimilation, model development and computational resources, the skill of the operational models have improved over the years. Prasad et al., (2011) demonstrated the improved skill of Global Forecasting System (GFS) T574L64 (~27 km) as compared to coarser resolution T382L64 (~38 km) model over the ISM region. Further, Prasad et al., (2014) reported that GFS T574L64 model exhibited one day gain in forecast skill as compared to T382L64 model configuration. Another recent study by Mukhopadhyay et al., (2019) clearly brings out the fidelity of operational GFS semi-Lagrangian (SL) T1534L64 (~12.5 km) model for the year of 2016-2017 summer monsoon over the Indian region. They have noted that the high-resolution GFS is able to predict the rainfall and associated large-scale dynamical parameters reasonably well. However, it is found that the forecasted rainfall appears to grossly overestimate over the Indian landmass, Arabian Sea and southern part of Bay of Bengal (BoB) region for different lead

time in their study. Further, the rainfall probability distribution function (PDF) showed an overestimation (underestimation) of lighter (heavier) rainfall for all the lead time over the ISM region. Finally, Mukhopadhyay et al., (2019) concluded that although GFS T1534 has shown reasonable fidelity in capturing the spatio-temporal variability of the ISM features, further development is required to enhance the forecast skill of heavy rainfall with a longer lead time.

Keeping the above issues of operational GFS T1534 in mind, a recent study by Ganai et al., (2019) examined the impact of modified rate of fractional cloud condensate to precipitation conversion parameter in the revised simplified Arakawa-Schubert (SAS) convection scheme in Climate Forecast System version 2 (CFSv2) in simulating ISM. The modified conversion parameter (C_0) is defined following Han et al., (2016) as

$$C_0 = a\exp[b(T - T_0)]\, for T \leq T_0, \qquad (1a)$$

$$C_0 = a \;\; for\, T > T_0, \qquad (1b)$$

where a (=0.002m^{-1}) and b (=0.07) are constants, T_0 (=0°C) is the freezing temperature and T is the atmospheric temperature. The C_0 is defined as a constant (0.002 m^{-1}) in default revised SAS. The exponential function of modified C_0 is derived following the results from a cloud resolving model simulation by Lim, (2011). Further details about the C_0 can be found in Lim, (2011); Han et al., (2016) and Ganai et al., (2019). Ganai et al., (2019) demonstrated that modified conversion parameter in revised SAS in CFSv2 shows considerable improvements in simulating mean ISM precipitation, outgoing longwave radiation (OLR), wind circulation, dynamical and thermodynamical processes etc. They have suggested that reduced rate of conversion of cloud condensate to convective precipitation above the freezing level leads to decrease in convective rainfall, which further enhances the detrained moisture from the upper-troposphere, resulting

enhancement in large-scale rainfall. Better simulation of convective and large-scale precipitation has resulted in improved total precipitation distribution over the ISM domain in CFSv2 in Ganai et al. (2019). Although Ganai et al. (2019) have assessed the fidelity of the climate model CFSv2 in detail over the ISM region, they have noted the potential of the modified C_0 in revised SAS convection scheme in predicting an extreme precipitation event over Mumbai in high resolution operational forecast model (GFS T1534). It is worth to mention that Han et al., (2016) have demonstrated the improved simulation of heavy precipitation event over Korea with modified conversion parameter in operational Global/Regional Integrated Model System (GRIMs) (Hong et al., 2013). They have suggested better model performance due to the decrease in convective precipitation from cloud condensate at colder temperature. Another recent study by Han et al., (2017) have shown the impact of modified C_0 in the operational NCEP GFS along with other updates in the convection scheme and indicated considerable improvement in summer precipitation over the continental USA.

While the above two studies (Han et al., 2016; Han et al., 2017) clearly demonstrated the importance of modified conversion parameter in the operational weather forecast model, it is remained to be seen its impact over the ISM region. It is already mentioned that Ganai et al., (2019) demonstrated the capability of modified C_0 in simulating one heavy precipitation event over Mumbai in GFS T1534. Additionally, Mukhopadhyay et al. (2019) have echoed to improve the forecast skill of heavy rainfall in operational weather forecast model (GFS T1534) over Indian region. Therefore, the primary objective of the present study is to assess the impact of modified C_0 in revised SAS convective scheme in GFS T1534 operational weather forecast model over the Indian summer monsoon region.

2. Model description, data and methodology

Presently, NCEP GFS version 14.1.0 with spectral resolution of T1534 (~12.5 km) with 64 hybrid sigma-pressure levels (top layer 0.27 hPa) is utilized for daily operational forecast over the ISM region. It is worth to mention that the present version of the operational GFS model is implemented from 2018 summer monsoon season replacing the older version (GFS version 13.0.2; Mukhopadhyay et al., 2019) over the Indian region. The dynamical core of the present high resolution deterministic model is based on a two-level semi-implicit Semi-Lagrangian (SL) discretisation approach (Sela, 2010), while the physics is carried out in the linear, reduced Gaussian grid in the horizontal space. The GFS version 14.1.0 uses various physics packages as described in table 1. With the increase in model resolution, NCEP GFS incorporated scale awareness following Arakawa and Wu, (2013) in the SAS deep and shallow convection scheme (Han and Pan, 2011; Han et al., 2017). In the SAS deep convection scheme (Han and Pan, 2011; Han et al., 2017), the cloud condensate to precipitation conversion parameter (C_0) is assumed to be a constant (0.002 m^{-1}) indicating the rate of generation of rainfall from cloud condensate is same from all the levels. However, recent study by Han et al., (2016) and Ganai et al., (2019) showed that the modified C_0 varies according to equations 1a and 1b based on the study by Lim (2011). In the present study, two separate GFS T1534 model forecasts are utilized, one with default version of convection scheme (CTRL hereafter) and the other with modified conversion parameter (C_0) (EXPT hereafter). Similar to Mukhopadhyay et al., (2019), the model forecast is run daily for 10 days (240hour) and the output is saved every 3 hour interval at 12.5 km regular grid. In the present manuscript, the two years (2018 and 2019) of forecast data for the summer monsoon season (June to September, JJAS) is used. Except the modified C_0 in EXPT, the other components of the GFS T1534 are kept unchanged for both the forecast run. Both the forecast runs are carried out at the Ministry of Earth Sciences high performance computing facility

154 "Pratyush" at the Indian Institute of Tropical Meteorology (IITM), Pune, India. The initial
155 conditions for the forecast are generated by NCMRWF through the NCEP-based ensemble
156 Kalman filter (EnKF) component of hybrid global data assimilation system (GDAS) cycle which
157 has more Indian data in it. Further details about the NCMRWF data assimilation system is
158 reported by Prasad et al., (2016).

159 To validate the model forecast, the daily observed gridded rainfall data at 25 km resolution is
160 utilized from India Meteorological Department (IMD) for the summer season of 2018 and 2019.
161 These data are merged product of gridded rain gauge observations and Global Precipitation
162 Measurement (GPM) satellite-estimated rainfall data over the ISM region (Mitra et al., 2014).
163 This dataset has been extensively used in several studies (Sridevi et al., 2019; Kar et al., 2018;
164 Prakash et al., 2016; Prasad et al., 2016; 2017 etc.) to validate the model forecast over Indian
165 region. In addition to rainfall, different satellite and reanalyses-based parameters are also used to
166 further analyze model performance. The fifth generation of ECMWF atmospheric reanalyses
167 (ERA5) products (Hersbach and Dee, 2016) is utilized at 25km horizontal resolution for the year
168 of 2018 and 2019 JJAS season. The satellite estimated outgoing longwave radiation (OLR) daily
169 data (Liebmann & Smith, 1996) from National Oceanic and Atmospheric Administration
170 (NOAA) is used in the present study.

171 In the present manuscript, the daily 24 hour accumulated rainfall is computed from 3 hourly (03
172 UTC of previous day to 03 UTC of forecast valid day) forecast data over the ISM domain for
173 both CTRL and EXPT. The rainfall time series is calculated for the JJAS season of the year of
174 2018 and 2019 for different lead times. The JJAS mean rainfall is calculated based on two years
175 of datasets for day-1, day-3, day-5 and day-8 forecast lead times. The spatial correlation
176 coefficient, root mean square error (RMSE), bias, rainfall probability distribution function

(PDF), easterly shear etc. are calculated for both observation and model forecast at various lead times.

3. Results and discussion

3.1. Seasonal mean precipitation and OLR distribution

We first investigate the model performance in capturing the seasonal (JJAS) mean rainfall distribution over the ISM region (Figure 1). The IMD-GPM merged data indicates that large amount of rainfall occurs over the Western Ghats, Bay of Bengal (BoB), northeast India and central Indian (CI) landmass region (Figure 1a). The southern peninsula and northwest India receives least amount of rainfall during summer monsoon season (Figure 1a). The large rainfall over the Western Ghats and northeast India is due to the topography over the regions (Rao, 1976). The biases in GFS T1534 with respect to observation are depicted in Figure 1b (CTRL) and Figure 1c (EXPT) respectively. Although the forecasts by both the model are able to capture the JJAS mean rainfall pattern reasonably at various lead times, some notable biases can be seen in both CTRL and EXPT. Both the models appear to grossly overestimate the rainfall over CI landmass region, northeast India, Himalayan foothills and Western Ghats region at various lead times (Figure 1b and 1c). However, the magnitude of rainfall overestimation gradually decreases with forecast lead days (day-3, day-5 and day-8). Mukhopadhyay et al., (2019) also showed similar results from older version of GFS T1534 over the ISM region during JJAS of 2016 and 2017. In addition, the northern (southern) part of BoB shows underestimation (overestimation) of rainfall amount in both the model forecasts at all the lead times. However, closer analyses reveal that with the modified conversion parameter forecast run (EXPT), the magnitude of the rainfall biases improved over the above regions as compared to CTRL forecasts at all the lead times

(Figure 1c). It is further evident from model to model comparison as in Figure 1d. Additionally, it is also established from various statistical parameters calculated over the all India land points as shown in table-2. The seasonal mean rainfall appears to be overestimated at all the lead time in CTRL forecasts whereas EXPT shows relative improvement as compared to observation (table 2). Additionally, the spatial correlation coefficient remains above 0.5 for all the lead times in both the model forecasts. Further, the RMSE appears to be slightly better in EXPT in day-1 forecast as compared to CTRL. However, with further lead times (day-3, day-5 and day-8), it is slightly better in CTRL forecast (table 2). On contrary, standard deviation analyses suggests that although the variability is slightly less in EXPT as compared to CTRL in day-1 lead time, EXPT shows better variability as compared to observation with further lead times (day-3, day-5 and day-8) over the continental Indian region. The above analyses bring out better rainfall fidelity with modified conversion parameter in GFS T1534 model over the Indian region. It is well documented that the revised SAS with constant C_0 has a tendency to produce more convective rainfall in global GCMs (Ganai et al., 2015; 2016; Saha et al., 2013) as well as in weather forecast models (Han et al., 2016; Han et al., 2017). In the modified C_0, the convective rainfall is decreased through the reduced rate of conversion of cloud condensate to convective precipitation above the freezing level, which further enhances the detrainment of condensate from convection in the upper level and resulted in an increase in large-scale precipitation (Han et al., 2016; Ganai et al., 2019). Thus, similar to CFSv2 in Ganai et al., (2019), it is possibly better simulation of convective and large-scale precipitation that may result in improving the total rainfall distribution in EXPT.

In order to find out the improvement in the total precipitation in EXPT forecast, the rainfall PDF is analyzed at different lead times for JJAS and different months of the summer season over the

continental India (Figure 2). The rainfall bins are taken according to Mukhopadhyay et al., (2019). The JJAS rainfall PDF (Figure 2a) reveals that both the models forecast overestimates the lighter (<1.56 cm/day) category rainfall at all the lead times. It is consistent with the study by Mukhopadhyay et al., (2019) where overestimation of lighter category rainfall is reported in GFS T1534 forecast. However, the GFS T1534 with modified C_0 forecast run shows considerable improvement in capturing moderate (1.56−6.45 cmday^{-1}), heavy (6.45−11.56 cmday^{-1}), very heavy (11.56−20.45 cmday^{-1}) and extreme (≥20.45 cmday^{-1}) category rainfall (Figure 2a, blue bars) as compared to observation at different lead times. On the other hand, CTRL forecast indicates gross overestimation over moderate category and underestimation of heavier category rainfall (Figure 2a, red bars). It further suggests that the total rainfall overestimation over Indian landmass in CTRL forecast is mainly due to excess contribution from lighter and moderate category rainfall. While Ganai et al., (2019) reported the importance of modified C_0 in GFS T1534 in capturing the heavy rainfall event over Mumbai, the present study further established the fact that the modified conversion parameter has the potential to improve the moderate to heavier category rainfall forecast over the ISM domain. To gain more insight about the rainfall PDF distribution during each month of JJAS, PDF analyses is carried out in Figure 2b to 2e. During June (Figure 2b), July (Figure 2c), August (Figure 2d) and September (Figure 2e), both the models exhibit similar PDF characteristics as seen in JJAS, particularly in July, August and September. The CTRL forecast appears to grossly overestimate (underestimate) the lighter to moderate (heavier) category rainfall whereas the EXPT shows overestimation of lighter category and considerable improvement in heavier category rainfall for all the lead times. On the other hand, during June, CTRL appears to perform better in forecasting moderate and very heavy category rainfall for day-1, day-3 and day-5 lead times as compared to EXPT (Figure 2b).

Similar results were also reported by Chakraborty, (2010) using ECMWF forecast data over ISM region.

In addition to rainfall PDF over continental India, it will be useful to investigate the spatial pattern of frequency of different categories of rainfall for various lead times over the ISM region (Figure 3). The spatial pattern depicts that both the models grossly overestimate the frequency of lighter rainfall (0.25- 2 cm/day) over the Indian landmass, BoB, Arabian Sea, Western Ghats and northeast India for all the lead time (day-1, day-3 and day-5) as shown in Figures 3b, 3c, 3d, 3e, 3f, and 3g. This is consistent with the rainfall PDF over the continental India as shown in Figure 2a. On the other hand, the frequency of moderate category (2-6 cm/day) rainfall shows considerable improvement over the central Indian landmass region in EXPT forecast for all the lead days (Figure 3c, 3e and 3g) as compared to observation (Figure 3a). On contrary, CTRL forecast shows large overestimation of moderate category rainfall over the central Indian landmass region (Figure 3b, 3d and 3f). This is contrary to the study by Mukhopadhyay et al., (2019) where they have shown (Figure 4 and 5 in their paper) underestimation of moderate rainfall in older version of GFS T1534. Further, it is noted that both the models overestimate the frequency of moderate rainfall over BoB, west coast and northeast Indian region. In addition to lighter and moderate rainfall, the frequency of heavy (6-10 cm/day) to very heavy category (>10 cm/day) rainfall indicates that both the models underestimate the frequency over the Indian landmass, BoB and Arabian Sea regions (Figure 3a to 3g) for the lead time. However, closer analyses reveal that EXPT forecast shows relative improvement in forecasting heavy to very heavy rainfall over central Indian landmass region (Figure 3c, 3e and 3f) as compared to CTRL forecast (Figure 3b, 3d and 3f). While the above analyses is consistent with the rainfall PDF

267 distribution over the continental India (Figure 2), the present analyses further bring out the
268 regional heterogeneities in frequency of different rainfall categories over the ISM domain.

269 The JJAS mean OLR bias is shown in Figure 4 for different lead times. The OLR bias depicts
270 that CTRL forecast overestimates over northern, northwestern India and BoB region as
271 compared to NOAA data. However, the magnitude of the biases slightly decreases with lead days
272 (Figure 4a). On contrary, EXPT forecasted OLR displays better distribution over the continental
273 Indian region for day-1 lead time (Figure 3b). The overestimation of OLR over the northern part
274 of India in CTRL is largely resolved in EXPT. However, the negative bias over the southern
275 peninsula and northeast India increases with further lead times as shown in Figure 4b. It is found
276 (Figure not shown) that modified conversion parameter enhances the detrainment of moisture in
277 the upper-troposphere leading to increase in upper level cloudiness and thus low OLR at the top
278 of the atmosphere is noted in EXPT. Similar decrease in OLR also reported by Han et al., (2016)
279 in Global/Regional Integrated Model system (GRIMs) over Korea. Moreover, Ganai et al.,
280 (2019) also reported slight underestimation of OLR at the top of the atmosphere over the ISM
281 region in CFSv2.

282 **3.2. JJAS Convective and Large-Scale Rainfall**

283 Han et al., (2016) and Ganai et al., (2019) have demonstrated that the modified C_0 tends to
284 reduce (enhance) the convective (large-scale) rainfall in weather and climate models
285 respectively. Keeping the above studies in mind, the impact of modified C_0 in operational GFS
286 T1534 is investigated in Figure 5. To define the convective and large-scale rainfall in GFS
287 T1534, similar methodology as in Ganai et al., (2019) is followed. The convective rainfall is
288 subtracted from the total rainfall to get the grid-scale or large-scale rainfall in the model. Here,

the comparison of convective and large-scale rainfall is made between the models only considering the fact that the definitions used to partition the convective and large-scale rainfall are different in observation and in model. The spatial distribution of convective (Figure 5a) and large-scale (Figure 5b) rainfall bias clearly demonstrates that the convective (large-scale) rainfall decreased (enhanced) over central India and northeast Indian region as compared to CTRL forecast for all the lead time. However, over the west coast, Arabian Sea and BoB, the magnitude of the convective rainfall is more in EXPT (Figure 5a). The improvement in different component of the total rainfall is further evident from the convective (large-scale) rainfall fraction over the continental Indian region as depicted in Figure 5c (5d). The CTRL forecast shows around 70% convective and 30% large-scale rainfall whereas in EXPT, it is around 60% (convective) and 40% (large-scale) for all the lead times. Therefore, the present analyses demonstrate the reduction of convective rainfall and enhancement in large-scale rainfall in EXPT forecast over continental India. Moreover, it also indicates that the improvement in total rainfall in EXPT is contributed by the proper representation of convective and large-scale rainfall over the ISM region.

3.3 Wind circulation

One of the major characteristic features of Indian summer monsoon is the presence of low-level (850 hPa) south westerly jet and upper-level (200 hPa) tropical easterly jet (Ramage, 1971; Rao, 1976) over the ISM domain. Both the low-level and upper-level circulation plays a crucial role in summer monsoon activity over the region. Both the models are able to capture the above wind circulations reasonably well (Figure 6) as compared to ERA5 for day-1 lead time. However, finer details reveal that the strength of the low-level south westerly and upper-level easterly jet over Indian landmass region is overestimated by 2-4 ms^{-1} in CTRL as compared to ERA5 reanalyses

(Figure 6a and 6c) for day-3, day-5 and day-8 lead time. It is possible that stronger low-level jet brings more moisture (Figure shown later) over the continental India which has resulted in rainfall overestimation in CTRL over the region. On the contrary, the strength of the above jets appears to be better resembled in EXPT as compared to ERA5 for all the lead times (Figure 6b and 6d). Although the strength of the south westerly and easterly jets are better captured in EXPT over the Indian landmass region, the low-level (upper-level) jet is found to be slightly overestimated (underestimated) over the equatorial Indian Ocean region for all the lead days. Consistent with the better wind circulation at 850 hPa and 200 hPa over Indian landmass region in EXPT, the easterly shear (difference between zonal wind at 200 and 850 hPa) shows considerable improvement as compared to ERA5 over the ISM region as shown in Figure 7b. It is worth to mention that easterly wind shear plays an important role for northward propagation of monsoon intraseasonal oscillation (Jiang et al., 2004). Figure 7a indicates that CTRL forecast is able to predict the shear reasonably well for day-1 lead time, however, with further lead times (day-3, day-5 and day-8), the shear appears to be underestimated over the Indian landmass (15°N-25°N) region. On the other hand, EXPT is able to predict proper easterly wind shear over the above region for all the lead times. Overall, the above analyses suggest that EXPT is able to predict better large-scale monsoonal wind circulation due to better large-scale heating associated with large-scale rainfall over the ISM region.

3.4. Evaluation of dynamical and thermodynamical processes

In order to evaluate the processes responsible for better model forecast with modified C_0in GFS T1534, various dynamical and thermodynamical processes are investigated over the central Indian landmass region. Both the models show overestimation of vertical motion for day-1 lead time from 900hPa and above as compared to ERA5 as depicted in Figure 8a. However, for day-3

lead time the vertical velocity slightly underestimates in both the models. Additionally, the magnitude of the vertical velocity suggests relative improvement in EXPT as compared to CTRL throughout the troposphere for day-1 and day-3 lead (Figure 8a).Consistent with stronger low-level wind circulation, the vertical profile of moisture convergence shows slight overestimation in the lower level in both the models for day-1 lead time (Figure 8b). However, EXPT forecast indicates relative improvement over CTRL for day-1 lead time. Since the modified C_0 forecast shows better performance in predicting large-scale rainfall and wind circulation over the ISM domain, it will be worth to evaluate the large-scale heating distribution over the region (Figure 8c). The large-scale apparent heat source (Q1) is computed following Yanai et al., (1973).The CTRL forecast produces stronger heating due to cumulus induced subsidence above 800 hPa as compared to ERA5 for day-1 lead time. On contrary, EXPT resembles better with ERA5 where the convective heating is decreased throughout the troposphere (Figure 8c). Similar results were also shown by Han et al., (2016) with GRIMs model. For day-3 lead time, both the models appear to slightly underestimate the heating at 800-300hPa but marginal improvement can be noted in EXPT as compared to ERA5 (Figure 8c). It is likely that in EXPT relatively improved vertical motion resulted from lower and middle level moisture convergence leading to enhanced detrainment of moisture from the upper level, which in turn increases the large-scale rainfall and influences the associated large-scale heating distribution.

In order to further gain insight about the rainfall and moist-convective processes, the vertical profile of relative humidity as a function of rain rate is analyzed during JJAS of 2018-2019 (Figure 9a-9b). The bias analyses reveals that CTRL forecasts have a systematic underestimation of lower-level moisture over the central Indian landmass region for all the lead time (Figure 9a). Similar underestimation of lower-level moisture was also reported by Mukhopadhyay et al.,

(2019) in older version of GFS T1534 over the region. In contrast, EXPT suggests relative improvement in lower-level moisture distribution for all the lead time over the central India region (Figure 9b). However, the upper-troposphere appears to be moister in EXPT due to the detrained moisture from the upper level in the modified scheme. Further, it is worth to mention that the lower-level moisture plays an important role in triggering, sustaining and maintaining the growth of the convective system. Hence, it is likely that better lower-level moistening in EXPT has resulted in realistic moist-convective feedback in the atmosphere. Moreover, to gain further understanding about the lower-level stability, the vertical profile of temperature as a function of rain rate is showed in Figure 10a-10b. Consistent with Figure 9b, the lower troposphere is relatively cooler in EXPT (Figure 10b) as compared to CTRL forecast (Figure 10a) due to more evaporation of large-scale precipitation for all the lead time. It further enhances the moisture in the lower troposphere and makes the atmosphere conducive for convection. These results are consistent with the previous studies with modified C_0 (Han et al., 2016; Ganai et al., 2019). The analyses in the present section bring out the better model fidelity with modified conversion parameter in representing large-scale heating and dynamical processes, which eventually improve the precipitation distribution over continental India.

3.5 Verification of model forecast

In order to further investigate the forecast skill of EXPT objectively, various skill scores are computed in the present section. We first calculate the Bias score (B) and Equitable Threat Score (ETS) based on a contingency table. This contingency table categorizes the observation and forecast into hits, ‘a’, false alarms, ‘b’, miss, ‘c’ and correct negatives ‘d’ with respect to a particular threshold. Based on these categories the Bias Score and ETS is calculated (Wilks 2011).

$$B = \frac{a+b}{a+c} \qquad (2)$$

$$ETS = \frac{a-a_{ref}}{a+b+c-a_{ref}} \qquad (3)$$

Figure 11a-d shows the Bias Score and Figure 11e-h shows the ETS for Day 1 to Day 4 rainfall forecast respectively. A Bias Score of 1 indicates a perfect forecast, greater than 1 indicates overforecasting and less than 1 indicates underforecasting. The EXPT shows a better Bias score than CTRL consistently for all lead time, although we find some over forecasting in case of EXPT for higher thresholds in case of Day 2. Another point of note is the better performance of EXPT for higher thresholds even at Day 4 lead time. In case of ETS, a score of 1 indicates a perfect forecast. In Figure 11e-h we can clearly see that the CTRL is marginally better than EXPT for 2cm/day threshold for all lead times but EXPT fares consistently better than CTRL for higher thresholds at all lead times. This indicates EXPT to have a better forecast skill than CTRL.

Further we also quantify the difference between CTRL and EXPT by calculating the Root Mean Square Error (RMSE) with respect to reanalysis for zonal (U) and meridional (V) wind forecast at 850 hPa and 200 hPa (Figure 12a-b). Overall the RMSE increases with lead time for both U and V wind. The RMSE at 200 hPa is higher than at 850 hPa. Though the CTRL and EXPT show similar behaviour, EXPT does not deteriorate further from CTRL and shows better RMSE for U200 indicating a better simulation of the Tropical Easterly Jet (TEJ) during monsoon season (Figure 6d).

Lastly, to better elaborate on the performance of both CTRL and EXPT with respect to rainfall forecast for JJAS season, “Chiclet diagram” (Carbin et al., 2016; Wang et al., 2017; Ganai et al.,

2019) is displayed over central India landmass region in Figure 13 for the summer monsoon of 2019. The usefulness of "Chiclet diagram" has been echoed by Wang et al., (2017) and Ganai et al., (2019) in CFSv2 and GFS T1534 respectively. It is evident from Figure 13a and 13b that both the models are showing similar pattern over the central India region. Moreover, detailed analyses reveal that for the first week of July both the models underestimated the heavy rainfall amount over central India in day-2 to day-8 lead time as compared to observation. On the contrary, for the month of August and September, EXPT (Figure 13b) shows notable improvement in terms of predicting magnitude of the rainfall amount for all the lead times as compared to CTRL (Figure 13a). From mid of August, CTRL shows systematic positive bias in rainfall amount for all the lead time and it has been largely resolved in EXPT.

4. Summary and conclusions

The present manuscript evaluated the performance of operational high resolution (~12.5 km) deterministic weather forecast model GFS T1534 with modified rate of cloud condensate to precipitation conversion parameter (C_0) in the SAS convection parameterization scheme for two summer monsoon seasons of 2018 and 2019 over the ISM region. While Ganai et al., (2019) has demonstrated the impact of modified C_0 in climate model CFSv2 in simulating the monsoon features over India, the present study deals with the impact of the same modification in operational forecasting system. The forecast evaluation indicates that EXPT shows better fidelity in capturing the mean rainfall over Indian landmass region for all the lead time as compared to CTRL. However, systematic prominent positive biases over west coast, northeast India and southern BoB remain in EXPT which needs further improvement. The rainfall PDF analysis indicates notable improvement in forecasting moderate and heavier category rainfall in EXPT as compared to CTRL which shows gross underestimation of the above category rainfall. However,

it is found that the modified C_0 appears to slightly overestimate the lighter category rainfall over continental India region. Further, the above findings are also established from the spatial map of different category-wise rainfall over the ISM domain.

The improvement in the total rainfall is appeared to be contributed by proper representation of convective and large-scale rainfall over the ISM region. Similar to climate model (CFSv2), the enhancement (decrease) of large-scale (convective) rainfall is noted in EXPT as compared to CTRL. The reduced rate of conversion of cloud condensate to convective precipitation in modified C_0 above the freezing level leads to increase in detrainment of moisture in the upper troposphere resulting in an increase in large-scale precipitation. As the upper level cloudiness increases due the above process, the OLR at the top of the atmosphere is slightly decreased in EXPT. Moreover, the wind circulation features shows improved pattern in EXPT over ISM region for all the lead time. It is possibly the improved heating distribution throughout the troposphere has resulted in realistic circulation over the ISM region. In addition to dynamical and thermodynamical processes, the lower tropospheric moistening is improved in EXPT as compared to CTRL for all the lead time. Finally, the model skill score analyses demonstrated that the skill of the model relatively improved for heavier category rainfall over the continental Indian region for all the lead time.

The present study clearly brings out the better model fidelity with modified conversion parameter in forecasting the moderate and heavy category rainfall over Indian region. Several studies have shown increasing trend in heavy rainfall over continental Indian region and also in recent years heavy rainfall events over Mumbai, Kerala, Uttarakhand and many other parts of the country causes severe damage to the livelihood of the region. Therefore, in order to improve the forecast of heavy rainfall, the modified C_0 can be incorporated in the present operational weather

forecast model. Moreover, it will be interesting to see in future works, the impact of the modified convection scheme in the operational extended range (4 weeks in advance) and seasonal forecast system over India. Although in the present study we have mainly focused on the mean features in the daily to seasonal scale, in future studies we will look into the sub-daily or diurnal scale features over ISM domain.

Acknowledgement

The Indian Institute of Tropical Meteorology (Pune, India) is fully funded by the Ministry of Earth Sciences, Government of India, NewDelhi. We would like to thank ECMWF for providing ERA5 data set (https://www.ecmwf.int/en/forecasts/datasets/reanalysis-datasets/era5). OLR data are accessed from http://www.esrl.noaa.gov/psd/data/gridded/data.interp_OLR.html#detail website. We thank IMD for providing the IMD-GPM merged data. All model runs are carried out on Pratyush High Performance Computing (HPC) system at Indian Institute of Tropical Meteorology (IITM), Pune, India. Authors (from IITM) thank Director, IITM, Pune for motivation and encouragement in the study.

List of Figures

Figure 1. (a) JJAS mean rainfall ($mmday^{-1}$) of IMD-GPM merged data during 2018-2019. The rainfall bias in (b) CTRL and (c) EXPT with respect to observation, (d) in EXPT with respect to CTRL for day-1, day-3, day-5 and day-8 lead times are shown.

Figure 2. All India rainfall PDF (%) vs. rain rate ($cmday^{-1}$) categories during (a) JJAS, (b) June, (c) July, (d) August and (e) September for different lead times derived from CTRL and EXPT forecast and compared with IMD-GPM merged gridded data.

Figure 3. Spatial distribution of rainfall frequency (%) for different rain rate ($cmday^{-1}$) categories during JJAS for (a) IMD-GPM merged data, (b, d and f) for CTRL and (c, e and g) for EXPT for different lead times.

Figure 4. Spatial distribution of OLR bias (Wm^{-2}) in (a) CTRL and (b) EXPT with respect to satellite based NOAA observation at day-1, day-3, day-5 and day-8 lead time during JJAS of 2018-2019.

Figure 5. Spatial distribution of (a) convective rainfall ($mmday^{-1}$) and (b) large-scale rainfall ($mmday^{-1}$) in EXPT with respect to CTRL for different lead times. (c) and (d) denote convective and large-scale rain fraction over continental Indian region for various lead days respectively.

Figure 6. Spatial distribution of wind circulation bias (ms^{-1}) in (a) CTRL and (b) EXPT with respect to ERA5 reanalyses at day-1, day-3, day-5 and day-8 lead time at 850 hPa level. (c) and (d) represent similar analyses but for 200 hPa pressure level.

Figure 7. Easterly zonal wind shear (ms^{-1}) (U200–U850) during JJAS as obtained from (a) CTRL and (b) EXPT at various lead times and compared with ERA5.

Figure 8. JJAS mean vertical profiles of (a) vertical velocity ($hPas^{-1}$), (b) moisture convergence (gm/kgs^{-1}) and (c) apparent heat source (Q1) ($Kday^{-1}$) for ERA5 (black line), CTRL (red line) and EXPT (blue line) for day-1 and day-3 lead times over the central Indian landmass region.

Figure 9. Vertical profile of bias in relative humidity (shaded in %) as a function of rain rate ($mmday^{-1}$) in (a) CTRL and (b) EXPT with respect to observation (ERA5 vs. IMD-GPM merged data) over the central Indian landmass region during JJAS of 2018–2019 at different lead times.

Figure 10. Vertical profile of bias in temperature (shaded in K) as a function of rain rate ($mmday^{-1}$) in (a) CTRL and (b) EXPT with respect to observation (NOAA vs. IMD-GPM merged data) over the central Indian landmass region during JJAS of 2018–2019 at different lead times.

Figure 11. RMSE of (a) U component of wind (ms^{-1})at 850 hPa (solid) and at 200 hPa (dashed) for CTRL (red line) and EXPT (blue line), (b) represents similar analysis but for V component of wind for JJAS 2018–2019 over the continental India.

Figure 12. (a-d) represent Bias score for CTRL (red bar) and EXPT (blue bar) for day-1 to day-4 lead days respectively over continental Indian region during JJAS of 2018-2019. (e-h) represent ETS score for CTRL (red bar) and EXPT (blue bar) for day-1 to day-4 lead time respectively. X-axis represents various rainfall thresholds ($cmday^{-1}$).

Figure 13. Chiclet diagram of daily precipitation bias ($cmday^{-1}$) in (a) CTRL and in (b) EXPT with respect to observation as a function of the verification date (x axis) and lead time (y axis) over central Indian region. Time series of daily mean precipitation ($cmday^{-1}$) is plotted in the lower panel in each plot.

List of tables

Table 1: Model physics in operational GFS T1534

Table 2: Various statistics (mean, spatial correlation coefficient (CC), root mean square error (RMSE), standard deviation) are calculated based on observed and model forecasted rainfall over continental Indian region for different lead time.

References

Abhik, S., Halder, M., Mukhopadhyay, P., Jiang, X., & Goswami, B. N. (2014). Possible new mechanism for northward propagation of boreal summer intraseasonal oscillations based on TRMM and MERRA reanalysis. Climate Dynamics, 40(7-8), 1611–1624. https://doi.org/10.1007/s00382-012-1425-x

Arakawa, A., & C.-M. Wu. (2013). A unified representation of deep moist convection in numerical modeling of the atmosphere. Part I. J Atmos Sci, 70, 1977–1992. https://doi.org/10.1175/JAS-D-12-0330.1.

Carbin, G. W., Tippett, M. K., Lillo, S. P., & Brooks, H. E. (2016). Visualizing long-range severe thunderstorm environment guidance from CFSv2. Bulletin of the American Meteorological Society, 97(6), 1021–1031. https://doi.org/10.1175/BAMS-D-14-00136.1

Chakraborty, A. (2010) The skill of ECMWF medium range forecasts during the year of tropical convection 2008. Mon Weather Rev, 138, 3787–3805.

Clough, S. A., Shephard, M. W., Mlawer, E. J., Delamere, J. S., Iacono, M. J., Cady-Pereira, K., et al. (2005). Atmospheric radiative transfer modeling: a summary of the AER codes. Journal of Quantitative Spectroscopy and Radiative Transfer, 91(2), 233–244. https://doi.org/10.1016/j.jqsrt.2004.05.058

Dirmeyer, P.A., Cash, B.A., Kinter, J.L. et al. Simulating the diurnal cycle of rainfall in global climate models: resolution versus parameterization. Clim Dyn 39, 399–418 (2012). https://doi.org/10.1007/s00382-011-1127-9

Gadgil, S., & Gadgil, S. (2006). The Indian monsoon, GDP and agriculture. Economic and Political Weekly, 41, 4887–4895.

Gadgil, S., & Sajani, S. (1998). Monsoon precipitation in the AMIP runs. Climate Dynamics, 14(9), 659–689. https://doi.org/10.1007/s003820050248

Ganai, M., Krishna, R. P. M., Mukhopadhyay, P., & Mahakur, M. (2016). The impact of revised siplified Arakawa-Schubert scheme on the simulation of mean and diurnal variability associated with active and break phases of Indian Summer Monsoon using CFSv2. Journal of Geophysical Research: Atmospheres, 121, 9301–9323. https://doi.org/10.1002/2016JD025393

Ganai, M., Krishna, R. P. M., Tirkey, Snehlata, Mukhopadhyay, P., Mahakur, M., & Han, J-Y. (2019). The Impact of Modified Fractional Cloud Condensate to Precipitation Conversion Parameter in Revised Simplified Arakawa-Schubert Convection Parameterization Scheme on the Simulation of Indian Summer Monsoon and Its Forecast Application on an Extreme Rainfall Event Over Mumbai. 124, 5379-5399. https://doi.org/10.1029/2019JD030278.

Ganai, M., Mukhopadhyay, P., Phani, R. M. K., & Mahakur, M. (2015). Impact of revised simplified Arakawa-Schubert convection parameterization scheme in CFSv2 on the simulation of the Indian summer monsoon. Climate Dynamics, 45(3-4), 881–902. https://doi.org/10.1007/s00382-014-2320-4

Goswami, B. N., Venugopal, V., Sengupta, D., Madhusoodanan, M. S., & Xavier, P. K. (2006). Increasing trend of extreme rain events over India in a warming environment. Science, 314(5804), 1442–1445. https://doi.org/10.1126/science.1132027

Hack, J. J., Caron, J. M., Danabasoglu, G., Oleson, K. W., Bitz, C., & Truesdale, J. (2006). CCSM–CAM3 climate simulation sensitivity to changes in horizontal resolution. J Climate, 19, 2267–2289.

Han, J., & Pan, H.-L. (2011). Revision of convection and vertical diffusion schemes in the NCEP global forecast system. Weather Forecasting, 26(4), 520–533. https://doi.org/10.1175/WAF-D-10-05038.1

Han, J., Wang, W., Kwon, Y. C., Hong, S.-Y., Tallapragada, V., & Yang, F. (2017). Updates in the NCEP GFS cumulus convection schemes with scale and aerosol awareness. Weather and Forecasting, 32(5), 2005–2017. https://doi.org/10.1175/WAF-D-17-0046.1

Han, J.-Y., Hong, S.-Y., Lim, K.-S. S., & Han, J. (2016). Sensitivity of a cumulus parameterization scheme to precipitation production representation and its impact on a heavy rain event over Korea. Monthly Weather Review, 144(6), 2125–2135. https://doi.org/10.1175/MWR-D-15-0255.1

Hersbach, H. & D. Dee (2016). ERA5 reanalysis is in production, ECMWF Newsletter No. 147, 7.

564 Hong, S.-Y., & Coauthors (2013). The Global/Regional Integrated Model System (GRIMs).
565 Asia-Pac. J Atmos Sci, 49, 219–243. doi:10.1007/s13143-013-0023-0.

566 Iacono, M. J., Mlawer, E. J., Clough, S. A., & Morcrette, J.-J. (2000). Impact of an improved
567 longwave radiation model, RRTM, on the energy budget and thermodynamic properties of the
568 NCAR Community Climate Model, CCM3. Journal of Geophysical Research, 105(D11),
569 14,873–14,890. https://doi.org/10.1029/2000JD900091

570 Jiang, X., Li, T., & Wang, B. (2004). Structures and mechanisms of the northward propagating
571 boreal summer intraseasonal oscillation. Journal of Climate, 17(5), 1022–1039.
572 https://doi.org/10.1175/1520-0442(2004)017<1022:SAMOTN>2.0.CO;2

573 Kar, S. C., Joshi, S., Shrivastava, S., & Tiwari, S. (2018). Dynamical characteristics of forecast
574 errors in the NCMRWF unified model (NCUM). Climate Dynamics. https
575 ://doi.org/10.1007/s0038 2-018-4428-4

576 Kiehl, J. T., & Williamson, D. L. (1991). Dependence of cloud amount on horizontal resolution
577 in the National Center for Atmospheric Research Community Climate Model. J Geophys Res,
578 96, 10 955-10 980

579 Kim, H-M., Webster, P. J., & Curry, J. A. (2012). Seasonal prediction skill of ECMWF system 4
580 and NCEP CFSv2 retrospective forecast for the Northern Hemisphere Winter. Climate
581 Dynamics, 39, 2957–2973. doi:10.1007/s00382-012-1364-6

582 Kim, I. W., Oh, J., Woo, S., & Kripalani, R. H. (2018). Evaluation of precipitation extremes over
583 the Asian domain: Observation and modelling studies. Climate Dynamics,
584 https://doi.org/10.1007/s00382-018-4193-4.

585 Liebmann, B., & Smith, C. A. (1996). Description of a complete (interpolated) outgoing
586 longwave radiation dataset. Bulletin of the American Meteorological Society, 77, 1275–1277.

587 Lim, K.-S. S. (2011). Investigation of aerosol indirect effects on simulated moist convections,
588 (PhD dissertation, 186 pp.). Yonsei University, Seoul, South Korea.

589 Lin, J.-L., K. M. Weickman, G. N. Kiladis, B. E. Mapes, S. D. Schubert, M. J. Suarez, J. T.
590 Bacmeister, & M.-I. Lee (2008), Subseasonal variability associated with Asian summer monsoon

591 simulated by 14 IPCC AR4 coupled GCMs, J. Clim., 21, 4541–4567,
592 doi:10.1175/2008JCLI1816.1.

593 Mahlman, J. D. , & Umscheid, L.J. (1987). Comprehensive modeling of the middle atmosphere:
594 the influence of resolution. In: Visconti G, Garcia R (eds) Transport process in the middle
595 atmosphere. D. Reidel, Hingham, MA, pp 251-266

596 Manabe, S., Smagorinsky, J., Holloway, J. L., & Stone, H. M. (1970). Simulated climatology of
597 a general circulation model with a hydrologic cycle. III: Effects of increased horizontal
598 computational resolution. Mon Weather Rev, 98, 175-212

599 Manganello, J. V., Hodge, K. I., & Kinter, J. L., et al. (2012). Tropical cyclone climatology in a
600 10-km global atmospheric GCM: Toward weather-resolving climate modeling. J Climate, 25,
601 3867–3893.

602 Mitra, A. K., Prakash, S., Imranali, M. M., Pai, D. S., & Srivastava, A. K. (2014). Daily merged
603 satellite gauge real-time rainfall dataset for Indian Region. Vayumandal, 40(1–4), 33–43.

604 Mukhopadhyay, P., & Coauthors (2019). Performance of a very high-resolution global
605 forecast system model (GFS T1534) at 12.5 km over the Indian region during the 2016–2017
606 monsoon seasons. Journal of Earth System Science, 128, 1-18, DOI:10.1007/s12040-019-
607 1186-6

608 Pan, H. L., & Wu, W. S. (1995). Implementing a mass flux convective parameterization package
609 for the NMC medium-range forecast model NMC Office Note. 409 (40 pp.).

610 Pattanaik, D. R., & Kumar, A. (2010). Prediction of summer monsoon rainfall over India using
611 the NCEP climate forecast system. Climate Dynamics, 34(4), 557–572.
612 https://doi.org/10.1007/s00382-009-0648-y

613 Prakash, S., Mitra, A. K., Momin, I. M., Rajagopal, E. N., Milton, S. F., & Martin GM (2016)
614 Skill of short to medium range monsoon rainfall forecasts from two global models over India for
615 hydro-meteorological applications. Meteorol Appl 23:574–586

616 Prasad, V. S., Johny, C. J., & Sodhi, J. S. (2016) Impact of 3D Var GSI-ENKF hybrid data
617 assimilation system. J Earth System Science, 125(8), 1509–1521.

Prasad, V. S., Johny, C. J., Mali, P., Singh, S. K., & Rajagopal, E. N. (2017) Retrospective analysis of NGFS for the years 2000–2011. Current Science, 112(2), 370–377.

Prasad, V. S., Mohandas, S., Das Gupta, M., Rajagopal, E. N., & Datta, S. K. (2011) Implementation of upgraded global forecasting systems (T382L64 and T574L64) at NCMRWF. NCMRWF Technical Report No. NCMR/TR/5/2011 May 2011, 72p, http://www.ncmrwf.gov.in/ncmrwf/gfs.report.final.pdf.

Prasad, V. S., Mohandas, S., Dutta, S. K., Das Gupta, M., Iyengar, G. R., Rajagopal, E. N., & Basu, S. (2014). Improvements in medium range weather forecasting system of India. J Earth System Science, 123(2), 247–258.

Rajeevan, M., Bhate, J., & Jaswal, A. K. (2008). Analysis of variability and trends of extreme rainfall events over India using 104 years of gridded daily rainfall data. Geophysical Research Letters, 35, L18707. https://doi.org/10.1029/2008GL035143

Rajendran, K., & Kitoh, A. (2008). Indian summer monsoon in future climate projection by a super high-resolution global model. Current Science, 95(11), 1560–1569.

Ramage, C.S. (1971). Monsoon Meteorology. Academic Press, New York, 296 p.

Ramu, D. A., Sabeerali, C. T., Chattopadhyay, R., Rao, D. N., George, G., Dhakate, A. R., et al. (2016). Indian summer monsoon rainfall simulation and prediction skill in the CFSv2 coupled model: Impact of atmospheric horizontal resolution. Journal of Geophysical Research: Atmospheres, 121, 2205–2221. https://doi.org/10.1002/2015JD024629

Rao, Y. P. (1976). Southwest monsoon, India Meteorological Department, Meteorological Monograph on Synoptic Meteorology. No. 111976, Delhi, p 337

Roxy, M. K., Ghosh, S., Pathak, A., Athulya, R., Mujumdar, M., Murtugudde, R., et al. (2017). A threefold rise in widespread extreme rain events over central India. Nature Communications, 8(1), 708. https://doi.org/10.1038/s41467-017-00744-9

Sabre, M., Hodges, K., Laval, K., Polcher, J., & Désalmand, F. (2000). Simulation of monsoon disturbances in the LMD GCM. Monthly Weather Review, 128(11), 3752–3771. https://doi.org/10.1175/1520-0493(2001)129<3752:SOMDIT>2.0.CO;2

Saha, S. K., Pokhrel, S., Chaudhari, H. S., Dhakate, A., Shewale, S., Sabeerali, C. T., et al. (2013). Improved simulation of Indian summer monsoon in latest NCEP climate forecast system free run. International Journal of Climatology, 34(5), 1628–1641. https://doi.org/10.1002/joc.3791

Sela, J. (2010). The derivation of sigma pressure hybrid coordinate semi-Lagrangian model equations for the GFS, NCEP Office Note 462, 31p.

Sperber, K. R., & Annamalai, H. (2008). Coupled model simulations of boreal summer intraseasonal (30–50 day) variability, Part 1: systematic errors and caution on use of metrics. Clim Dyn, 31, 345-372. doi:10.1007/s00382-008-0367-9

Sperber, K. R., & Palmer, T. N. (1996). Inter-annual tropical rainfall variability in general circulation model simulations associated with the atmospheric model inter-comparison project. Journal of Climate, 9(11), 2727–2750. https://doi.org/10.1175/1520-0442(1996)009<2727:ITRVIG>2.0.CO;2

Sridevi, C., Singh, K.K., Suneetha, P. et al. Rainfall forecasting skill of GFS model at T1534 and T574 resolution over India during the monsoon season. Meteorol Atmos Phys 132, 35–52 (2020). https://doi.org/10.1007/s00703-019-00672-x

Sundqvist, H., Berge, E., & Kristjansson, J. E. (1989). Condensation and cloud parameterization studies with a mesoscale numerical weather prediction model. Monthly Weather Review, 117, 1641–1657. https://doi.org/10.1175/1520-0493(1989)117<1641:CACPSW>2.0.CO;2

Waliser, D. E., Jin, K., Kang, I. S., Stern, W. F., Schubert, S. D., Wu, M. L. C., et al. (2003). AGCM simulations of intraseasonal variability associated with the Asian summer monsoon. Climate Dynamics, 21(5-6), 423–446. https://doi.org/10.1007/s00382-003-0337-1

Wang, S., Anichowski, A., Tippett, M. K., & Sobel, A. H. (2017). Seasonal noise versus subseasonal signal: Forecasts of California precipitation during the unusual winters of 2015-2016 and 2016-2017. Geophysical Research Letters, 44, 9513–9520. https://doi.org/10.1002/2017GL075052

671 Wilks, D. S. (2011). Statistical methods in atmospheric sciences. 3rd edn, International
672 Geophysics Series, No. 100, Academic Press, USA, 669p.

673 Williamson, D. L., Kiehl, J. T., & Hack, J. J. (1995). Climate sensitivity of the NCAR
674 community climate model (CCM2) to horizontal resolution. Climate Dynamics, 11, 377–397.

675 Yanai, M., Esbensen, S., & Chu, J.-H. (1973). Determination of bulk properties of tropical cloud
676 clusters from large-scale heat and moisture budgets. Journal of the Atmospheric Sciences, 30,
677 611–627. https://doi.org/10.1175/1520-0469(1973)030<0611:DOBPOT>2.0.CO;2

678 Yang, B., Fu, X., &Wang, B. (2008). Atmosphere-ocean conditions jointly guide convection of
679 the boreal summer intraseasonal oscillation: Satellite observations. Journal of Geophysical
680 Research, 113, D11105. https://doi.org/10.1029/2007JD009276

681 Zhao, Q., & Carr, F. H. (1997). A prognostic cloud scheme for operational NWP models.
682 Monthly Weather Review, 125(8), 1931–1953.
683 https://doi.org/10.1175/1520-0493(1997)125<1931:APCSFO>2.0.CO;2

Table 1. Model physics in operational GFS T1534

Physics	**Description**
Convection	Revised simplified Arakawa-Schubert deep convection (Pan and Wu, 1995; Han and Pan, 2011, Han et al., 2017) and mass flux based SAS shallow convection (Han and Pan, 2011) with Arakawa and Wu, (2013) scale-aware parameterization
Cloud Microphysics	Zhao and Carr, (1997), Sundqvist et al., (1989) formulated grid-scale condensation and precipitation
Gravity Wave Drag (GWD)	GWD based on Alpert et al., 1988; Kim and Arakawa, (1995), Mountain blocking (Lott and Miller, 1997) and stationary convective-forced GWD (Chun and Baik 1998)
PBL	Hybrid Eddy-diffusivity Mass flux vertical turbulent mixing scheme (Han and Pan, 2011; Han et al. 2015)
Radiation	Shortwave and Longwave radiation based on Rapid Radiative Transfer Model (RRTM) (Iacono et al., 2008; Clough etal., 2005) with Monte Carlo Independent Column Approximation (McICA).

Figure 1.

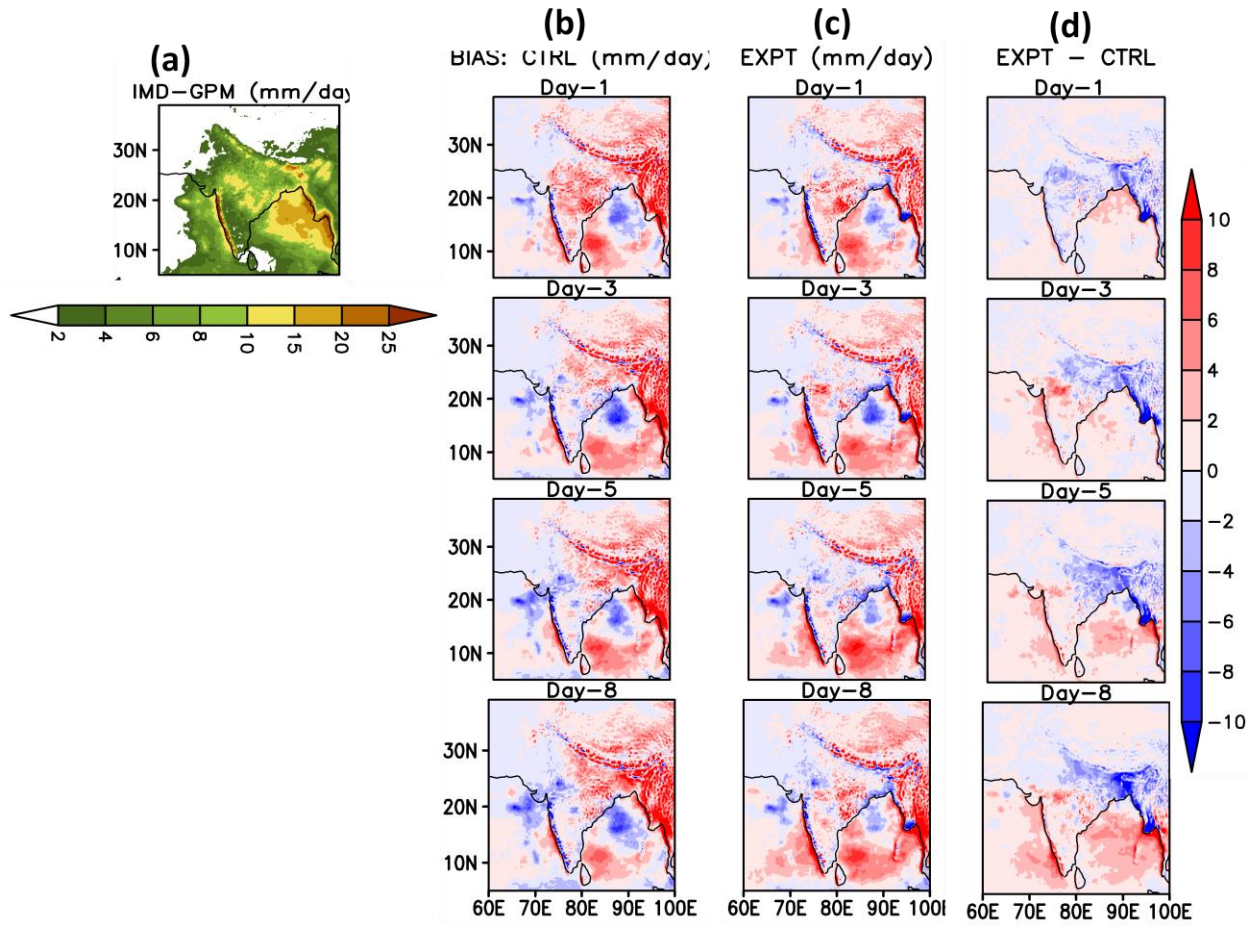

Figure 1. (a) JJAS mean rainfall ($mmday^{-1}$) of IMD-GPM merged data during 2018-2019. The rainfall bias in (b) CTRL and (c) EXPT with respect to observation, (d) in EXPT with respect to CTRL for day-1, day-3, day-5 and day-8 lead times are shown.

Table 2. Various statistics (mean, spatial correlation coefficient (CC), root mean square error (RMSE), standard deviation) are calculated based on observed and model forecasted rainfall over continental Indian region for different lead time.

	Lead day	Mean (mm/day)	CC	RMSE (mm/day)	Standard deviation (mm/day)
IMD-GPM		7.1			14.9
CTRL	Day-1	9.2	0.56	16.7	12.7
EXPT	Day-1	8.2	0.51	16.5	12.3
CTRL	Day-3	7.6	0.56	17.2	11.6
EXPT	Day-3	7.4	0.55	17.7	12.3
CTRL	Day-5	7.6	0.54	17.9	11.4
EXPT	Day-5	6.9	0.53	18.0	11.5
CTRL	Day-8	7.9	0.54	18.5	11.2
EXPT	Day-8	7.5	0.56	18.7	11.7

Figure 2.

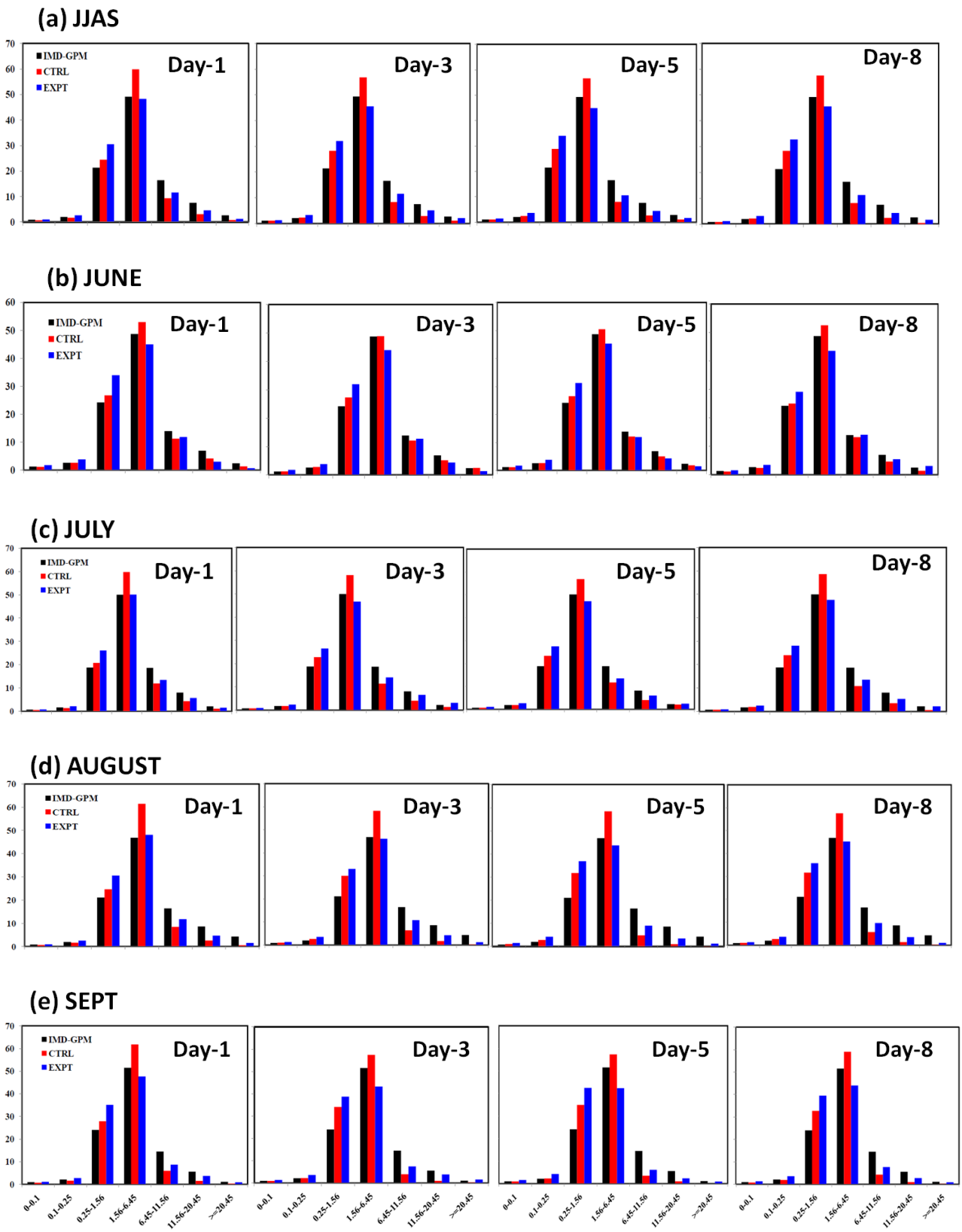
(a) JJAS
(b) JUNE
(c) JULY
(d) AUGUST
(e) SEPT
IMD-GPM
CTRL
EXPT
Day-1
Day-3
Day-5
Day-8
0-0.1
0.1-0.25
0.25-1.56
1.56-6.45
6.45-11.56
11.56-20.45
>=20.45

Figure 2. All India rainfall PDF (%) vs. rain rate ($cmday^{-1}$) categories during (a) JJAS, (b) June, (c) July, (d) August and (e) September for different lead times derived from CTRL and EXPT forecast and compared with IMD-GPM merged gridded data.

Figure 3.

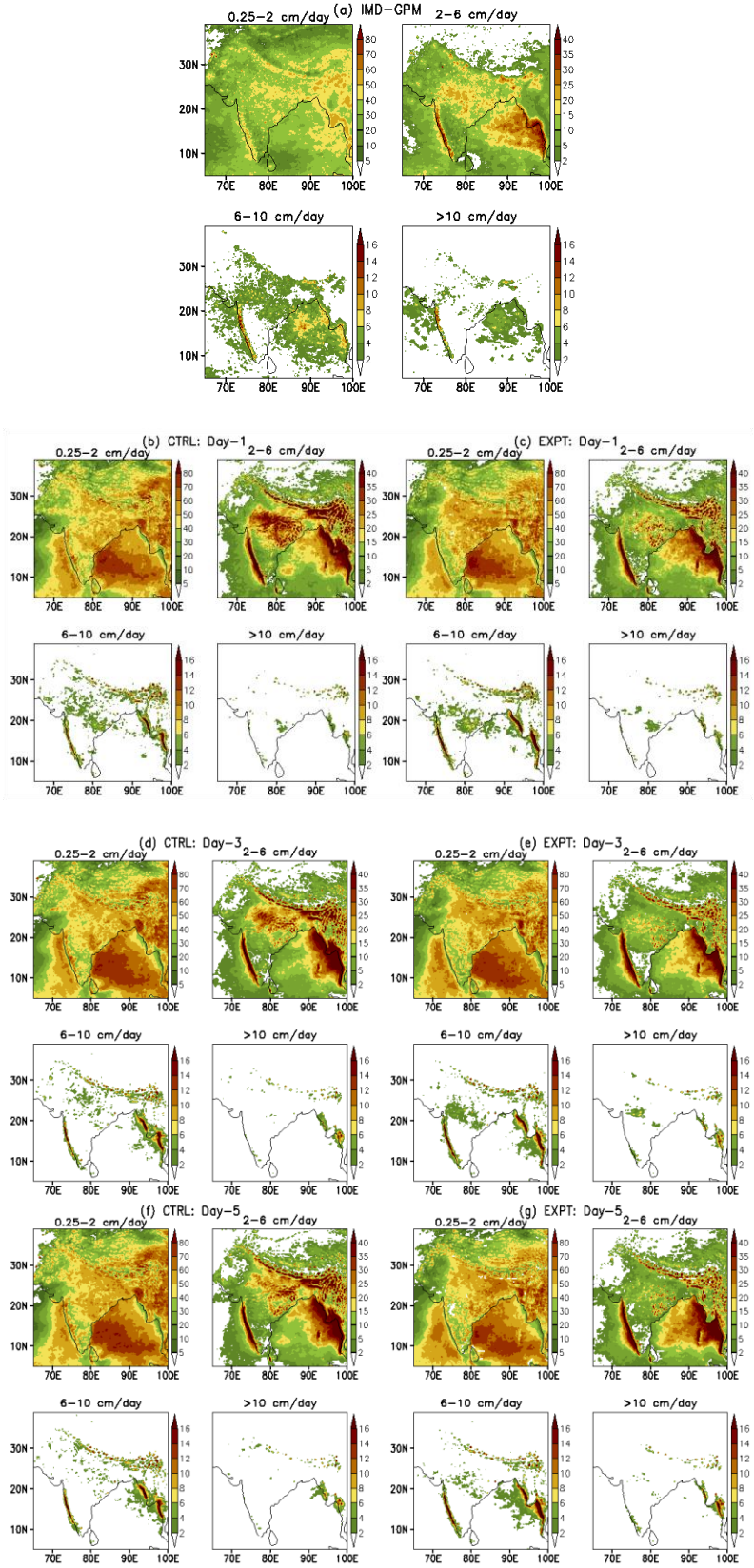
(a) IMD–GPM
0.25–2 cm/day
2–6 cm/day
6–10 cm/day
>10 cm/day
(b) CTRL: Day–1
(c) EXPT: Day–1
(d) CTRL: Day–3
(e) EXPT: Day–3
(f) CTRL: Day–5
(g) EXPT: Day–5
30N
20N
10N
70E
80E
90E
100E

Figure 3. Spatial distribution of rainfall frequency (%) for different rain rate ($cmday^{-1}$) categories during JJAS for (a) IMD-GPM merged data, (b, d and f) for CTRL and (c, e and g) for EXPT for different lead times.

Figure 4.

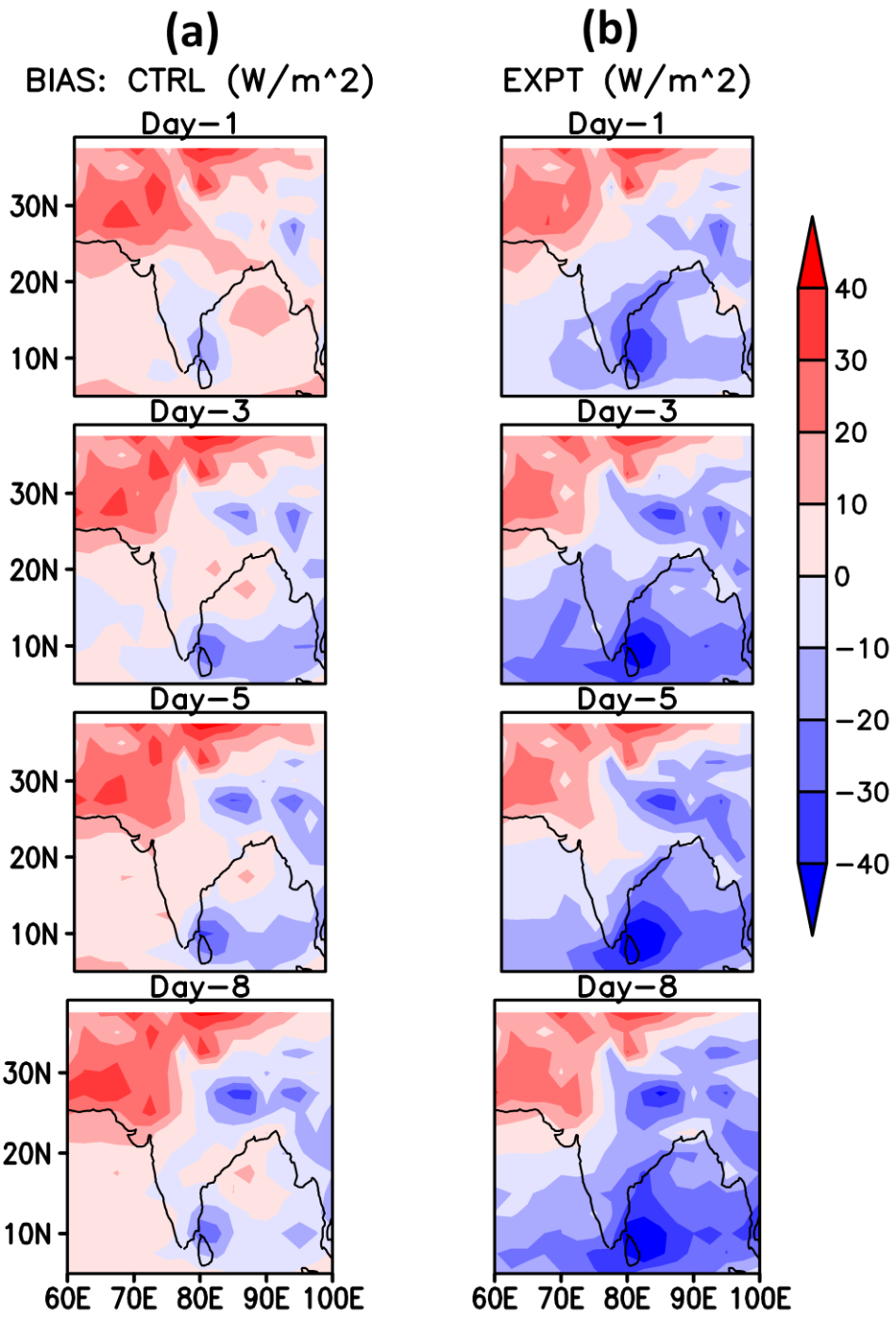

Figure 4. Spatial distribution of OLR bias (Wm^{-2}) in (a) CTRL and (b) EXPT with respect to satellite based NOAA observation at day-1, day-3, day-5 and day-8 lead time during JJAS of 2018-2019.

Figure 5.

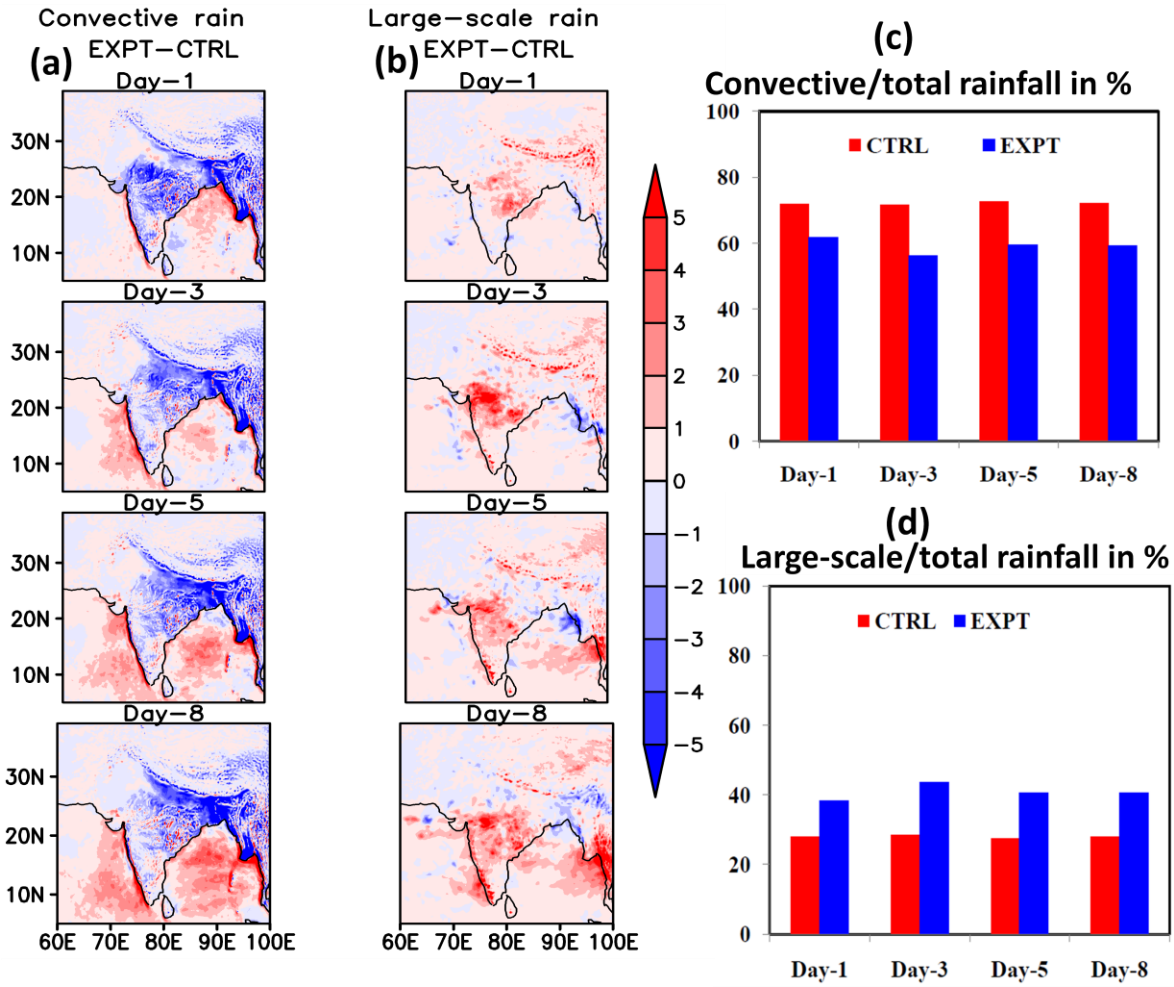

Figure 5. Spatial distribution of (a) convective rainfall (mmday^{-1}) and (b) large-scale rainfall (mmday^{-1}) in EXPT with respect to CTRL for different lead times. (c) and (d) denote convective and large-scale rain fraction over continental Indian region for various lead days respectively.

Figure 6.

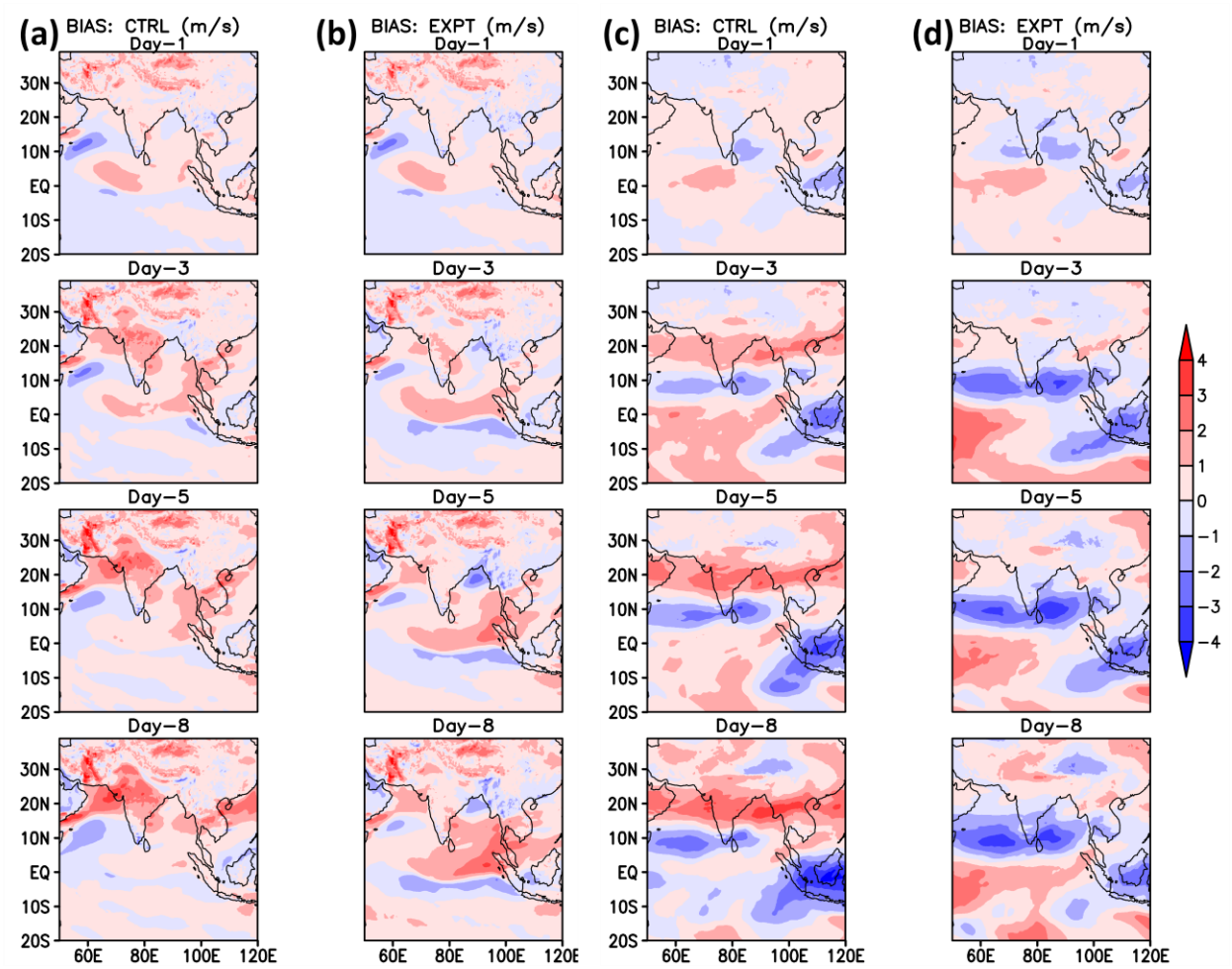

Figure 6. Spatial distribution of wind circulation bias (ms^{-1}) in (a) CTRL and (b) EXPT with respect to ERA5 reanalyses at day-1, day-3, day-5 and day-8 lead time at 850 hPa level. (c) and (d) represent similar analyses but for 200 hPa pressure level.

Figure 7.

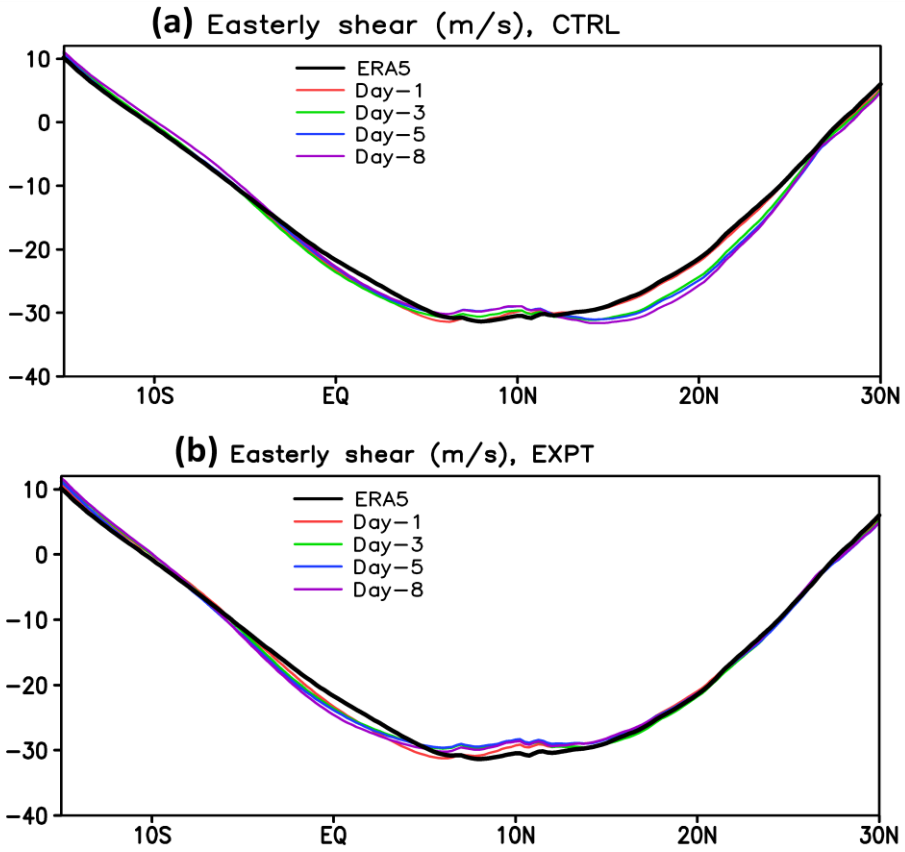

Figure 7. Easterly zonal wind shear (ms^{-1}) (U200–U850) during JJAS as obtained from (a) CTRL and (b) EXPT at various lead times and compared with ERA5.

Figure 8.

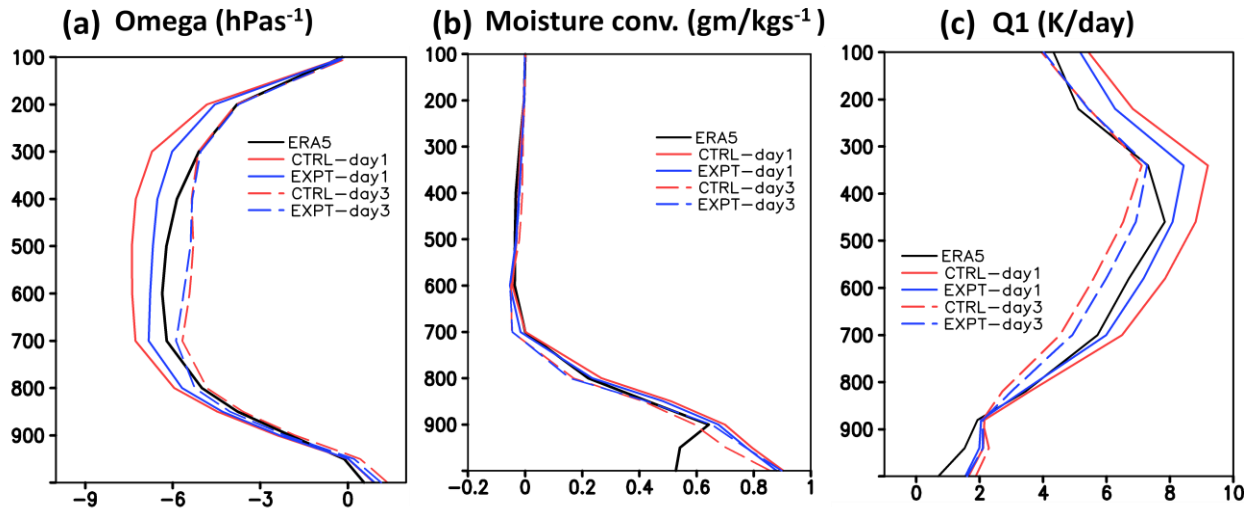

Figure 8. JJAS mean vertical profiles of (a) vertical velocity ($hPas^{-1}$), (b) moisture convergence (gm/kgs^{-1}) and (c) apparent heat source (Q1) ($Kday^{-1}$) for ERA5 (black line), CTRL (red line) and EXPT (blue line) for day-1 and day-3 lead times over the central Indian landmass region.

Figure 9.

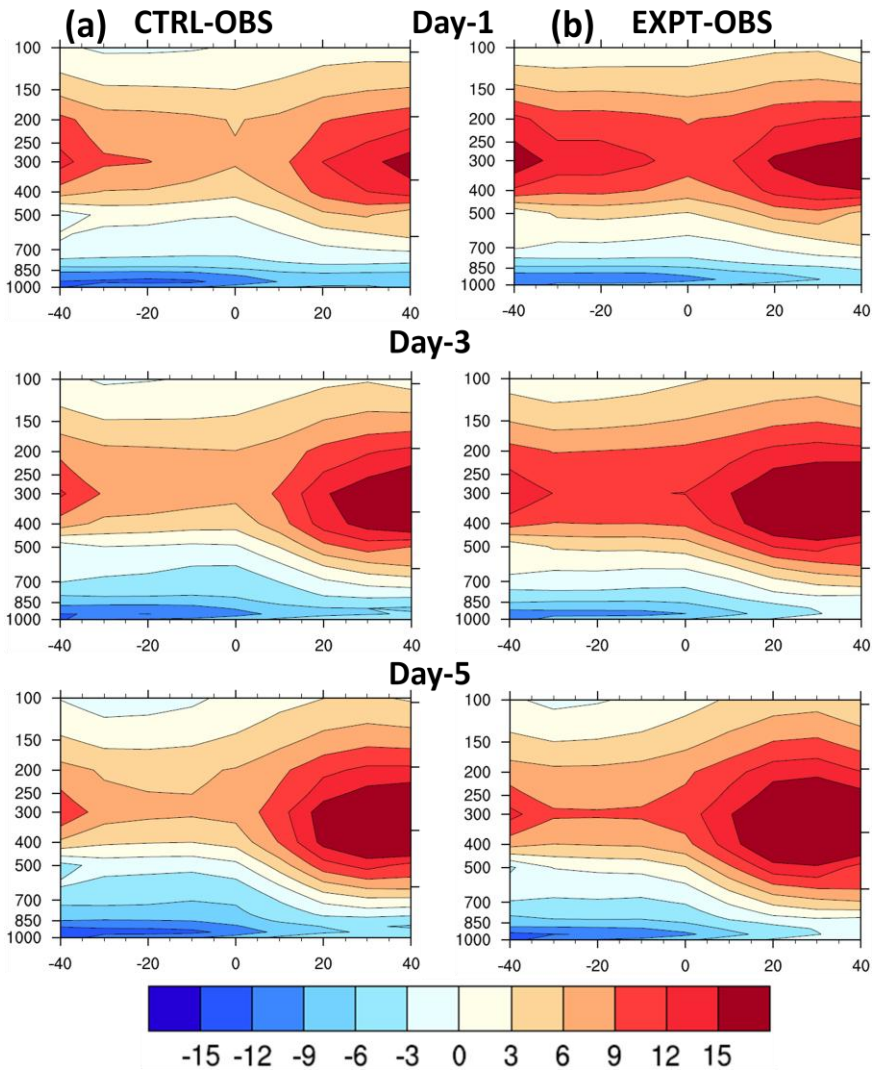

Figure 9. Vertical profile of bias in relative humidity (shaded in %) as a function of rain rate ($mmday^{-1}$) in (a) CTRL and (b) EXPT with respect to observation (ERA5 vs. IMD-GPM merged data) over the central Indian landmass region during JJAS of 2018–2019 at different lead times.

Figure 10.

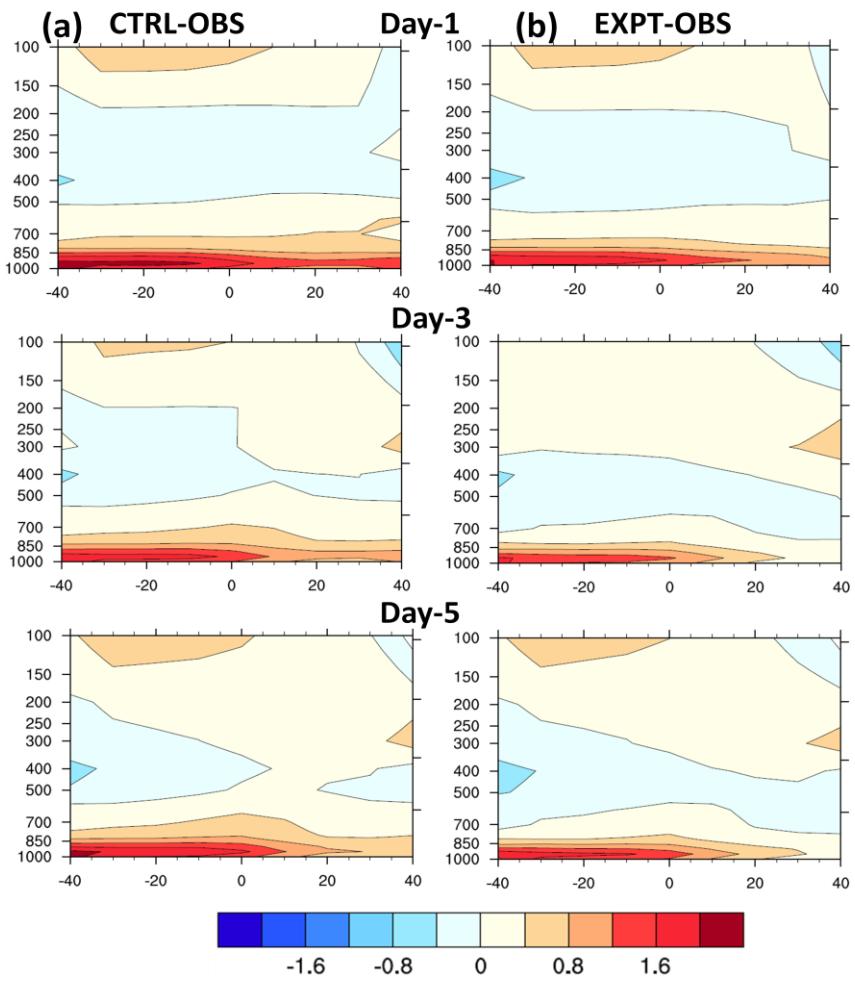

Figure 10. Vertical profile of bias in temperature (shaded in K) as a function of rain rate ($mmday^{-1}$) in (a) CTRL and (b) EXPT with respect to observation (NOAA vs. IMD-GPM merged data) over the central Indian landmass region during JJAS of 2018–2019 at different lead times.

Figure 11.

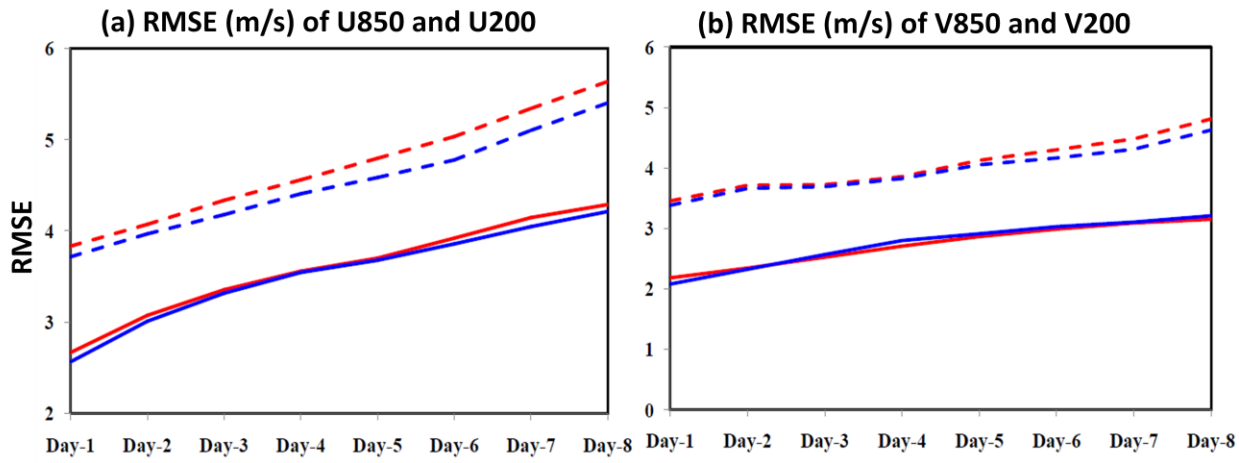

Figure 11. RMSE of (a) U component of wind (ms^{-1})at 850 hPa (solid) and at 200 hPa (dashed) for CTRL (red line) and EXPT (blue line), (b) represents similar analysis but for V component of wind for JJAS 2018–2019 over the continental India.

Figure 12.

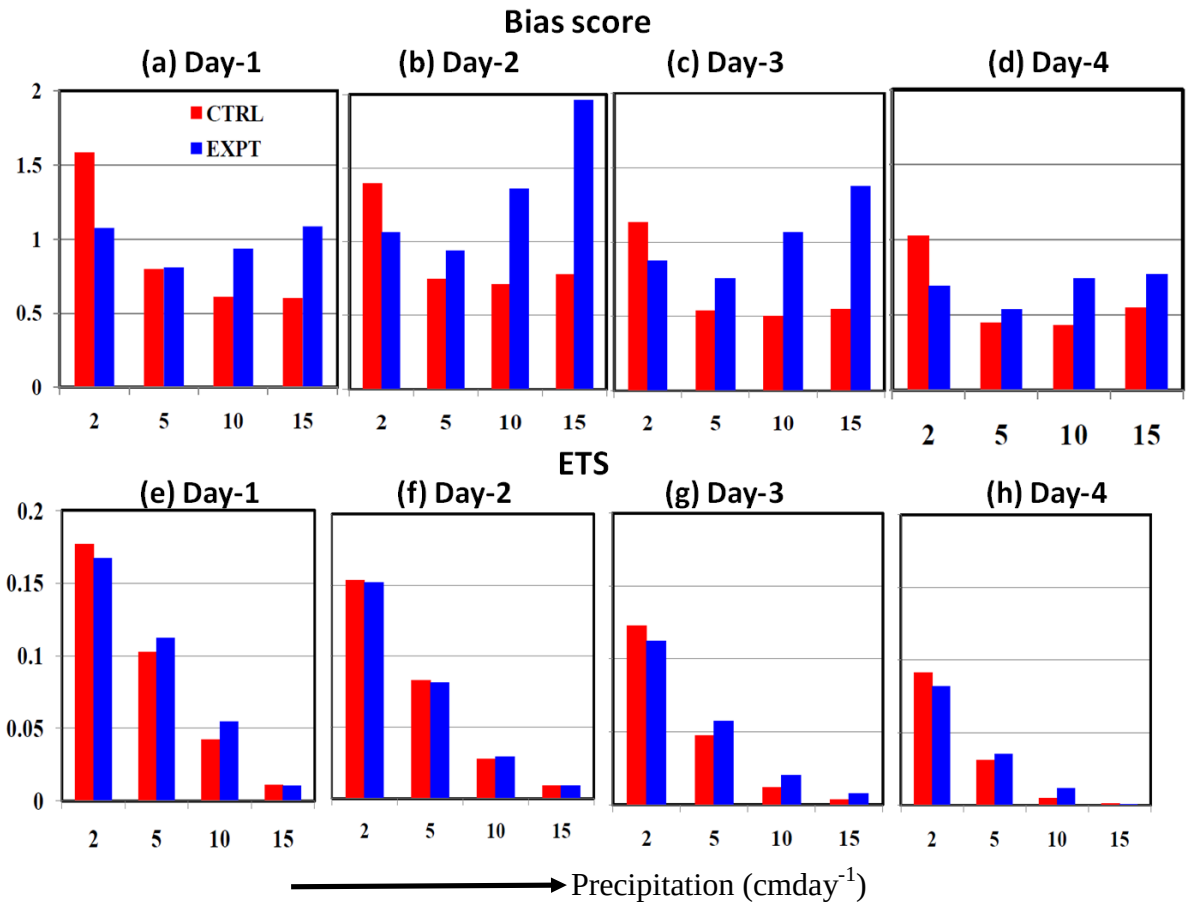

Figure 12. (a-d) represent Bias score for CTRL (red bar) and EXPT (blue bar) for day-1 to day-4 lead days respectively over continental Indian region during JJAS of 2018-2019. (e-h) represent ETS score for CTRL (red bar) and EXPT (blue bar) for day-1 to day-4 lead time respectively. X-axis represents various rainfall thresholds (cmday^{-1}).

Figure 13.

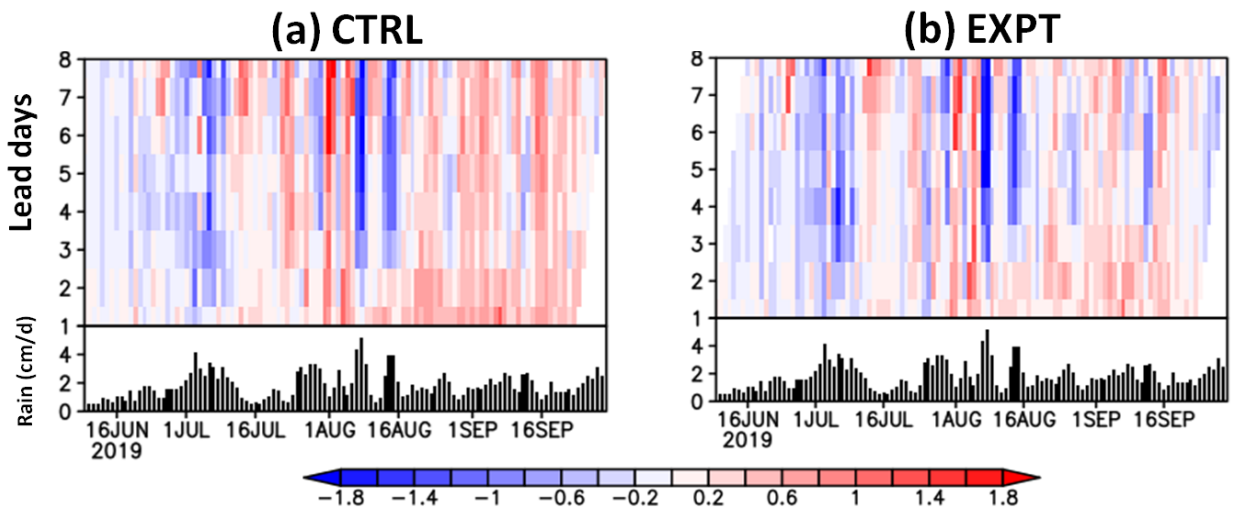

Figure 13. Chiclet diagram of daily precipitation bias (cmday^{-1}) in (a) CTRL and in (b) EXPT with respect to observation as a function of the verification date (x axis) and lead time (y axis) over central Indian region. Time series of daily mean precipitation (cmday^{-1}) is plotted in the lower panel in each plot.